



LAWRENCE
LIVERMORE
NATIONAL
LABORATORY

Standoff detection of oil and powder mixtures at 12 meters using a tunable quantum cascade laser-based system with a close focus telescope and uncooled infrared detector

J. C. Carter, P. H. Paul, J. M. Ottaway, P. Haugen, A. M. Manuel

November 1, 2021

Applied Spectroscopy

Disclaimer

This document was prepared as an account of work sponsored by an agency of the United States government. Neither the United States government nor Lawrence Livermore National Security, LLC, nor any of their employees makes any warranty, expressed or implied, or assumes any legal liability or responsibility for the accuracy, completeness, or usefulness of any information, apparatus, product, or process disclosed, or represents that its use would not infringe privately owned rights. Reference herein to any specific commercial product, process, or service by trade name, trademark, manufacturer, or otherwise does not necessarily constitute or imply its endorsement, recommendation, or favoring by the United States government or Lawrence Livermore National Security, LLC. The views and opinions of authors expressed herein do not necessarily state or reflect those of the United States government or Lawrence Livermore National Security, LLC, and shall not be used for advertising or product endorsement purposes.

Standoff detection of oil and powder mixtures at 12 meters using a tunable quantum cascade laser-based system with a close focus telescope and uncooled infrared detector

J. Chance Carter, Phillip H. Paul, Joshua M. Ottaway, Peter Haugen, Anastacia M. Manuel

Lawrence Livermore National Laboratory, 7000 East Ave., Livermore, CA, 94550, USA
(J.C.C., P.H.P., J.M.O., P.H., A.M.M.)

Abstract

We have designed and demonstrated a quantum cascade laser (QCL) based standoff system that utilizes an uncooled mercury cadmium telluride (MCT) detector with lock-in signal processing for chemical identification at a distance of 12.5 meters in indoor ambient light conditions. In the system, a tunable quad-QCL operating (1 MHz) in quasi-continuous wave mode between 8.45 to 10.03 μm (~ 1182 to 1000 cm^{-1}) serves as the active mid-infrared source for remotely interrogating mineral, powder, and thin film oil samples including powder mixtures (6%, 12.5%, 25%, 50%) of crystalline quartz (SiO_2) in KBr. Light as reflected from a given sample is collected using a 10-inch Dall Kirkham telescope and coupled via ZnSe optics to an uncooled MCT detector. The mixture dependence of the highly transparent KBr and strongly absorbing quartz was found to fit a modified version of the Schatz reflectance model for compacted powder mixtures. All reflectance spectra reported are relative to an Au-coated diffuse reflector. A NIST traceable polystyrene standard reflector was also used to determine the QCL wavelength tuning range and calibration.

Introduction

Standoff technologies are enabling new and exciting opportunities in exploration and measurement science. As of this writing – June 2021 – and approximately 343 million km from earth, NASA's Perseverance Rover¹, armed with a suit of analytical tools along with a helicopter and 20 plus cameras, is exploring the surface and atmosphere of Mars in the Jezero Crater. Onboard Perseverance is the SuperCam instrument² – a more advanced version of its technology predecessor, Curiosity's ChemCam instrument³ – which includes both Raman and Laser Induced Breakdown Spectroscopy (LIBS) standoff capabilities for analyzing the molecular and atomic composition of soils and rocks. With its range of 7 m, the laser housed in SuperCam is the key enabling subcomponent for performing Raman and LIBS measurements, remotely and in situ.

Quantum cascade lasers (QCLs) operating in the mid-infrared (mid-IR) represent an important evolving technology, enabling new and exciting opportunities in measurement science as well. QCLs are small, solid-state, linearly polarized infrared sources that are configurable as water or convection cooled, single or tunable wavelength systems. Commercial, high power, tunable QCLs are available in the 3.6 to 12 μm wavelength range with output powers up to 300 mW. The tuning range of a typical single QCL module is 10% of the center band frequency, so to cover a wide wavelength range, several tunable laser modules must be integrated into a single device. Such benchtop systems, which typically utilize external cavity QCLs with electromechanical actuated grating configurations for tuning, can rapidly tune in 100 ms over the entire wavelength range of the QCL module.

Although QCLs have yet to travel to another planet as part of a NASA exploration mission, there is great interest in the technology as investigators continue to advance its use in standoff applications involving chemical detection⁴⁻¹⁶ and as the technology continues to evolve. A recent innovation¹⁷ aimed at expanding the fieldability of QCLs is the development of electronically tuned, fast scanning QCLs. By replacing the electromechanical tuning component with an acousto-optical modulator (AOM), QCL tuning speeds between any two wavelengths is achieved in $<1 \mu\text{s}$ and involves no-moving parts in the system. This and other innovations are expanding the possibilities and application space of QCL technologies.

Here, we describe a standoff system utilizing a state-of-the-art, in terms of high power, external cavity QCL with electromechanical tuning integrated with a close focus Dall Kirkham telescope and coupled to an uncooled (i.e., no thermoelectric or liquid nitrogen cooling) MCT detector. The QCL-based standoff system described in this paper utilizes a lock-in-based detection scheme for measuring samples (minerals, oil, and powder mixtures) having high absorbance spectral features in the spectral region from ~ 1182 to 1000 cm^{-1} (8.45 to $10.03 \mu\text{m}$). The uncooled MCT detector produced good quality and suitable dynamic range reflectance data at a standoff distance of 12.5 m . The combination of a tunable QCL source modulated at high frequency with an uncooled detector and lock-in signal processing offers the potential for fieldable standoff applications involving chemical identification of neat or mixed compounds.

Experiment

Overview

The standoff system (Figure 1) comprises a telescope coupled to an MCT detector, a tunable QCL, and a controller and data acquisition system. During operation, collimated QCL pulses are aligned coaxially with the telescope field of view via two parallel 45° alignment mirrors (i.e., parallel Z-fold configuration) followed by an all reflective 2X beam expander (BX) and a 45° mirror (M1) mounted opposite the telescope secondary mirror. As shown in Figure 1, the optical path is mostly horizontal with an Au-coated, first surface, plane mirror (M2) set at 45° and mounted 1 m above the sample to direct the laser pulses downward so that samples could be mounted horizontally. Mirror M2 is $75 \times 75 \text{ mm}$ and sufficiently large compared to the QCL beam and telescope field of view (FOV) so that the telescope is the limiting aperture for light collection; M2 does not affect measurements other than signal losses associated with its Au coating. Light reflected from samples positioned 12.5 m away is collected by the telescope via mirror M2 and focused onto an MCT detector, which is capable of sampling each individual QCL pulse. The detector output is processed using a lock-in detection scheme. A more detailed discussion of the key subcomponents follows.

Telescope

The fully ruggedized, custom telescope (RC Optical Systems Inc., model 2005 carbon Dall Kirkham, 10-inch clear aperture, 2286 mm focal length, $f/9$, $\sim 40\%$ linear obscuration, protected Au coatings; Flagstaff, AZ, USA) is designed for close focus measurement of samples at distances of 10 to 50 m . The secondary mirror is mounted on an electromechanical actuator to enable focusing, which maintains the telescope back focus at 30.5 cm from the primary mirror. ZnSe optics serve to collimate (L1: Thorlabs, LF7113-F, $f = -150.0 \text{ mm}$; Newton, NJ, USA) and focus (L2: Thorlabs, AL72550-G, $f = 50 \text{ mm}$; Newton, NJ, USA) light onto the MCT detector. The telescope barrel-length was extended by 25 cm to accommodate a beam directing mirror (M1:

Thorlabs, PF20-03-M02; Newton, NJ, USA) positioned at a 45° angle and located opposite the telescope secondary mirror.

Quantum Cascade Laser (QCL)

Four integrated, high power, QCLs (Pranalytica Inc., Omnilux; Santa Monica, CA, USA) enable any combination of scanning across the wavelength range between ~ 4 to 10 μm with rapid tuning across the individual wavelength range of any single QCL module in 100 ms. For the studies described in this paper, only one of the four QCLs was utilized for standoff measurements. Specifically, the QCL tunable from 8.45 to 10.03 μm (~1182 to 1000 cm^{-1}) was operated with a maximum average power of 140 mW at the 9.4 μm center band frequency, a pulse duration of 300 ns at 1 MHz repetition rate, and a 350 ms tuning delay between scanned wavelengths. The QCL used in the present study employs an electromechanical actuator to tilt the grating to predetermined Littrow positions for tuning. The QCL generates two analog trigger outputs: a high frequency (1 MHz) TTL pulse train to trigger the pulse electronics to drive the individual lasers in quasi-continuous wave mode; and a gate trigger that indicates when a selected QCL module is tuning. The former trigger serves as the reference signal input to the lock-in amplifier (Stanford Research Systems, SR865; single channel, 2MHz-DSP; Sunnyvale, CA, USA). The amplified (Boston Electronics Corp., Vigo Systems, SIP-DC-10M-T039-NG; Brookline, MA, USA) signal from the MCT detector (Boston Electronics Corp., Vigo System, PVMI-10.6-1x1, maximum $D^* 7\text{E}+08 \text{ cm}^2\sqrt{\text{Hz}}/\text{W}^{-1}$ at 7.5 μm ; Brookline, MA, USA) is the input to the lock-in amplifier, which removes any detector offset. For all measurements, the voltage input range to the lock-in, which varied between 10 to 30 mV, was optimally set to ensure maximum signal gain without overloading. A time constant of 30 ms was used for all measurements with Gaussian 24 dB/oct finite impulse response (FIR) filtering. The 30 ms time constant in combination with the QCL wavelength tuning delay of 350 ms provided sufficient settling time for recording the phase magnitude independent R parameter from the lock-in via the embedded controller/chassis (National Instruments, PXI-8196/PXI-1042; Austin, TX, USA). This PC-based platform controls all aspects of the automated standoff measurements via custom Labview (National Instruments, 2017; Austin, TX, USA) code operating under Windows 7. The custom Labview interface enables the user to set experimental parameters (QCL selection, wavelength scanning range, resolution, wavelength dwell time) and monitor data acquisition in real time.

Telescope field of view / beam alignment

An optical fiber (Fiberguide Industries Inc., pure fused silica / silica clad, 0.22 NA, low OH; Caldwell, ID, USA), positioned one focal length away from lens L2 (Figure 1 inset, grey box), delivered a near-collimated beam of HeNe laser light (632 nm) to lens L1, and into the telescope to project an illuminated spot 12.5 m in front of the telescope. The broad transmission of ZnSe from the visible to mid-IR (~550 nm to 20 μm) enables using the same lens pair (L1 and L2) for retroreflecting HeNe light to establish the telescope FOV during initial alignment and for focusing mid-IR collected light onto the MCT detector during measurements. The optomechanical design at the rear of the telescope enables the option of switching between the MCT or optical fiber as needed. Once the telescope FOV is coarsely established, QCL pulses are directed onto the illuminated FOV to visibly optimize the overlap using thermal imaging paper (Edmund Scientific, #72-375, 20-25C Liquid Crystal Sheet; Barrington, NJ, USA). At a standoff distance of 12.5 m, the QCL beam size was slightly oval with the short and long diameters estimated to be 8 and 10 mm. The QCL pulses and telescope FOV overlap and FOV focus were optimized by adjusting

laser alignment mirrors and the telescope secondary mirror via a handheld controller, respectively, to achieve maximum collection of the signal as reflected from an Au-coated diffuse reflector (Thorlabs, DG10-120-M01; Newton, NJ, USA).

Data Handling

Data postprocessing was accomplished using a combination of Igor Pro (Wavemetrics, version 6.32A; Lake Oswego, OR, USA) and R (version 4.1.0) programming language.

Samples

All starting materials were used as received unless otherwise stated. A NIST traceable (NIST 1921b), mid-IR diffusely reflecting wavelength standard (Middleton Spectral Vision, MRC-910-1921GW, herein denoted as polystyrene standard reflector; Middleton, WI, USA) having sharp polystyrene spectral features across 8.45 to 10.03 μm (~ 1182 to 1000 cm^{-1}) served as a sample. Other samples chosen for measurements include olive oil (Bertolli extra virgin olive oil), high-purity quartz (SiO_2) crystal powder (AdValue Technology, 99.9% pure, SD-990; Tucson, AZ, USA), and potassium bromide (KBr) powder (Pike Technologies Inc., 160-8010; Fitchburg, WI, USA). The KBr average particle size distribution provided by the vendor is as follows: 150 - 75 μm (21.2%); 75 - 49 μm (23.5%); 49 - 45 μm (19.3%); finer than 45 μm (36%). The quartz powder average particle size distribution provided by the vendor (mean 105 μm volume %) is as follows: 350 - 250 μm (<5%); 250 - 50 μm (>94%); finer than 50 μm (<1%). Because of its strong absorption in the mid-IR, a thin layer of olive oil (<25 μm) was prepared in aluminum weigh dishes (Ward's Science, 470306-930; Rochester, NY, USA). The sample set also included an Au-coated diffuse reflector (Thorlabs, DG10-120-M01; Newton, NJ, USA), described by the vendor as a first-surface Au-coating over a 120-grit surface finish and having an average reflectance of coating of greater than 96% from 0.8 to 20 μm at 0 to 45° angle of incidence.

Sample mixtures

KBr and quartz powders were dried for 24 hours at 120°C with several stirrings of the powder to break up any small clumps, crusts, and layers over that time period. Approximately, 15-gram total mixtures by mass (6%, 12.5%, 25% and 50%) of quartz powder in KBr powder along with 100% KBr and 100% quartz powder samples were prepared in sealable polypropylene containers (Flackteck, Max 10 translucent cup, 501-226T; Landrum, SC, USA). Each ~15-gram mixture occupied between one-third to one-half the polypropylene container volume, which, based on experience, enables homogeneous powder mixing. The contents of the sealed polypropylene containers were mixed using resonant acoustic mixing (Resodyn Acoustic Mixer, LabRAM II, herein denoted as RAM; Butte, Montana, USA), which uses sound-induced oscillations of the container, up to many times the acceleration due to gravity (G), to create material movement and subsequent homogeneous mixing. The following RAM oscillation protocol was used: 50G for 15 sec; 90G for 30 sec (to break up any clumps that may have formed by absorption of water); 75G for 15 sec; and 50G for 30 sec. The individual ~15-gram samples of pure KBr and pure quartz powders were subjected to the same RAM mixing protocol. The RAM process produced a noticeable settling (~9 mm final thickness) of the powder bed in the cup. All prepared mixtures were stored in a glass desiccator when not in use. Note: Quartz and KBr powder particle sizes in the range used represent an inhalation hazard so proper precautions must be used in sample preparation to avoid inhaling or ingesting the powders.

Benchmark (non-standoff) instrumentation

An FT-IR spectrometer (Bruker Scientific LLC, Vertex 70; Billerica, MA, USA) was used to acquire transmittance measurements of olive oil and quartz powder samples for qualitative comparison with corresponding QCL-based standoff reflectance measurements. Bulk olive oil was measured in transmission mode using a demountable liquid cell (Pike Technologies, 162-1100, 160-1113 and 160-1112, 162-1230; Fitchburg, WI, USA) having 1.5 mm ZnSe windows and a 50- μm optical pathlength. To mitigate etalon effects when acquiring single scan background transmission spectra, a single 3 mm thick ZnSe window was measured instead of the empty liquid cell.

Attenuated total reflection (ATR) spectra of bulk quartz powder were acquired using a diamond crystal accessory (Bruker Scientific LLC, Platinum ATR; Billerica, MA, USA), having a single reflection (45° incidence angle) and a sampling area of 4.0 mm^2 ($2.0 \times 2.0\text{ mm}$). The resulting ATR spectrum was postprocessed by performing an ATR transformation using the extended ATR correction (Bruker Scientific LLC, OPUS 7.5.18; Billerica, MA, USA), which corrects for the wavelength dependent depth of penetration of the evanescent wave and anomalous dispersion caused by changes in the refractive index at or near strong absorption features. Essentially, this procedure corrects for distortions of relative line intensities and spectral shifts, so the ATR spectrum of the quartz powder sample is representative of a spectrum acquired in transmission measurement mode, provided the inputs for sample refractive index, ATR crystal refractive index, angle of incidence and number of light bounces are known.

Results and Discussion

The signal as reflected from a given sample may include Fresnel reflection, Reststrahlen reflection and transfection. Reflectance values are reported as the signal as reflected from a given sample divided by the signal as reflected from the Au-coated diffuse reflector. For all reflectance measurements reported herein, samples were placed at a standoff distance of 12.5 m and positioned horizontally and thus normal to the incident QCL beam. The QCL-based standoff system was preset to scan over the range from ~ 1182 to 1000 cm^{-1} (8.45 to $10.03\text{ }\mu\text{m}$) in increments of 0.2 cm^{-1} . This spectral range, which is relatively free of potential spectral interferences from water, required use of only one of the quad-QCL modules. To evaluate the tuning range of the factory calibrated QCL, standoff measurements were acquired of a polystyrene standard reflector, comprising a polystyrene thin film ($38\text{ }\mu\text{m}$ thickness) on an Au-coated diffusely reflecting substrate. The commercially available polystyrene standard reflector is traceable to a NIST infrared standard and is typically used in industry for calibrating instruments in the 714 to 1250 cm^{-1} (8 to $14\text{ }\mu\text{m}$) range. The effective optical pathlength of measured polystyrene is twice the film thickness since incident light is partially absorbed and transmitted and then reflected through the film where light is again partially absorbed and transmitted. Signal as reflected from the polystyrene standard reflector (Figure 2a, solid trace) is a combination of signal as reflected directly from the front surface of the polystyrene film (i.e., Fresnel) and signal as reflected from the underlying Au-coated diffusely reflecting substrate (i.e., transfection) with the latter expected to be higher. The signal as reflected from the Au-coated diffuse reflector, which is used in postprocessing to report reflectance values, is also shown in Figure 2a (dashed trace). The explanation for the greater signal from the polystyrene standard reflector versus the Au-coated diffuse reflector was not evaluated as part of this study but may be attributed to several factors and possibly a combination thereof including the latter having a more diffusely reflecting substrate.

The former, having a combined specular first-surface reflection from polystyrene with a less-diffuse transfection from the underlying Au-coated substrate, is another consideration. Refraction in the polystyrene film is another possible factor. The profile of the Figure 2a spectra result from the wavenumber dependent power output of the QCL across its tuning range, which is somewhat Gaussian, although a 6th order polynomial fit provides much improved agreement with the measured data (not shown).

The reflectance spectrum of Figure 2b, which shows three sharp absorption spectral features (labeled 1 - 3) for polystyrene, is the ratio of the signal as reflected by the polystyrene standard reflector (Figure 2a, solid trace) and the signal as reflected by the Au-coated diffuse reflector (Figure 2a, dashed trace). Plotting reflectance sufficiently removes the power output profile of the QCL. In addition, spectral features from ambient water (denoted by * in Figure 2a) resulting from QCL beam absorption at select wavenumbers over the roundtrip pathlength distance of 26 meters (12.5 m x 2) are sufficiently removed as shown in Figure 2b. This postprocessing does not appear to adversely affect the spectral features of polystyrene including the band at $\sim 1177\text{ cm}^{-1}$, which was not included in the NIST traceable data for the polystyrene standard reflector but has been reported by Ref 18. Finally, the differences in wavenumber position between the QCL factory calibration and the polystyrene standard reflector were $\sim 2\text{ cm}^{-1}$ with the QCL shifted to the low side of the certified wavenumber data provided by the manufacturer (Figure 2b, inset Table, Std. column). The cause, possibly Fresnel reflections from polystyrene or simply QCL calibration drift, was not investigated further since the differences were not sufficient to cause misidentification of the polystyrene spectral features.

Olive oil was selected as a liquid sample in this study for its strong absorption in the mid-IR and well-known band assignments¹⁹⁻²¹. The reflectance spectrum (Figure 3a) of a thin film olive oil sample is from measurements acquired with the QCL-based standoff system at a distance of 12.5 m. Similar to the polystyrene standard reflector measurement previously described, the signal as reflected from the olive oil is a combination of signal as reflected directly from the front surface of the olive oil film and signal as reflected from the underlying aluminum sample holder (i.e., transfection). The transmittance spectrum (Figure 3b), acquired with a benchtop FT-IR spectrometer, is included to show the overall breadth of the C-O vibrational region of olive oil, which extends beyond the tuning range of the QCL. As a visual aid for comparing spectra, three prominent absorption features are numerically labeled. The black solid trace in Figure 3a and the red solid trace in Figure 3b correspond to the same spectral range from $1176\text{ to }1000\text{ cm}^{-1}$. Differences in the relative appearance of the 1163 cm^{-1} band in Figure 3a and b are attributed to nearly all incident light being absorbed by the olive oil for the 1163 cm^{-1} transmission measurement, due to the use of a $50\text{ }\mu\text{m}$ optical pathlength cell²². Given the double-pass effect of the transfection measurement, the thickness of the thin film olive oil sample is less than $25\text{ }\mu\text{m}$ in the standoff measurement.

The reflectance spectrum of bulk quartz powder is shown in Figure 4 (black trace, left axis). The reflectance values plotted for quartz are the signal as reflected from the quartz powder divided by the signal as reflected from the Au-coated diffuse reflector, having an Au-coating over a 120-grit sandblasted surface (i.e., $102\text{ }\mu\text{m}$ average size), which corresponds to the mean quartz powder particle size. All quartz powder measurements using the standoff system were acquired at a distance of 12.5 m over the full range of the QCL ($1182\text{ to }1000\text{ cm}^{-1}$; $8.46\text{ to }10\text{ }\mu\text{m}$), which

corresponds to a portion of the spectral region (8 to 12 μm) where silicates such as quartz display Reststrahlen reflections²³. Reststrahlen bands occur when the imaginary part (k) of the refractive index is large such that very little energy passes through grain boundaries, and thus the scattering and absorption properties are controlled by first surface reflection and multiple scattering.²⁴ The transmittance spectrum (red trace, right axis) of bulk quartz powder includes strong absorption features associated with antisymmetric Si-O-Si stretching vibrations, which correspond to the Reststrahlen reflections. The spectral structure, relative band magnitudes and wavenumber offsets of reflectance and transmittance features presented in Figure 4 are consistent with spectra reported by Rost and coworkers²⁵ and Salisbury and coworkers^{26, 27}.

Figure 5 shows the real and imaginary parts of the refractive index for quartz taken from the measurements of Papova and coworkers²⁸. The strong resonance peak between 1111.1 and 1052.6 cm^{-1} is associated with the antisymmetric stretching vibration of Si-O-Si bridges.²⁹ The absorption coefficient (plotted in Figure 5 and computed as $\alpha = 4\pi k/\lambda$ with k the imaginary part of the index and λ the wavelength) is sufficiently large that any light entering a nominal 100- μm diameter quartz powder particle is substantially absorbed and not refracted. The Fresnel reflection at normal incidence is also plotted in Figure 5; the broad peak in Fresnel reflection centered at about 1120 cm^{-1} is due to Reststrahlen reflections in quartz.

Standoff measurements were performed on powders of 0, 6, 12.5, 25, 50 and 100% quartz in KBr by mass. The pure KBr sample is sufficiently transparent at the studied wavenumbers such that light reaching the polypropylene sample holder bottom surface may be reflected back through the sample. For the pure KBr, the relative reflectance (signal as reflected from the sample divided by signal as reflected from the Au-coated diffuse reflector) showed no spectral features and had a value of ~ 0.8 over the test wavenumber range.

Figure 6 shows the reflectance of various powder mixtures of quartz in KBr. The dip in relative reflectance seen at about 1156 cm^{-1} is associated with a gap between nearby vibrational modes.³¹ At 6% quartz, the mass weighted absorption coefficient of the mixture is greater than about 27 / mm (taking the absorption coefficient of KBr as negligible and taking 0.45 / μm as the absorption coefficient for quartz at $\sim 1000 \text{ cm}^{-1}$). Samples with 6% or more quartz and at all wavenumbers considered may then be treated as infinitely thick (i.e., any reflection from the far surface or from the sample holder is negligible). At the wavenumbers studied the relative reflectance decreases systematically in going from 6 to 50% quartz by mass. The 100% quartz powder sample follows this pattern except for wavenumbers of 1176.5 to 1162.8 cm^{-1} and 1149.4 to 1075.3 cm^{-1} ; in these ranges the reflectance from the 50 to 100% quartz powder mixtures increases rather than decreases systematically.

The mixture dependence of reflectance for powder mixtures of quartz in KBr was found to be well-approximated by the function

$$\ln R_\lambda = -b_\lambda(1 + c_\lambda x(1 - d_\lambda x)) \quad \text{Equation 1}$$

where R_λ is the reflectance at wavelength λ , x the mass fraction of quartz, with $c_\lambda \equiv 2b_\lambda + 3.2(1 - d_\lambda)$, and the values for b_λ and d_λ obtained from a non-linear-least-squares fit. Figure 7 shows the fitted reflectance as a function of mass fraction quartz for select wavenumbers.

Hecht^{30,31} reviewed several approaches to modeling the reflectance as a function of mixture. None of the forms considered by Hecht for a semi-infinite layer covers the range of functional behaviors observed in the quartz/KBr powder mixtures. Possibly the relationships considered are not appropriate to a mixture of one highly transparent with one strongly absorbing and scattering component (e.g., a classical dielectric material mixed with a component exhibiting Reststrahlen reflections).

Schatz³² considered compacted mixtures of ceramic and metal powders and reported measurements that covered wavelengths including strong resonance absorption in one of the components. The Schatz model may be better suited to the settled powdered beds produced by RAM mixing. For a mixture of component A transparent and component B strongly absorbing, Schatz suggests a mixture reflectance

$$R_{\text{mix},\lambda} = S_A^2 R_{A,\lambda} + S_A S_B R_{A,\lambda}^S + S_B R_{B,\lambda} \quad \text{Equation 2}$$

where R_A and R_B are the reflectance's of the pure components. Schatz describes R_A^S as the reflectance of an average particle of component A, when surrounded completely by particles of component B. The quantity S_B , given in Equation 3, is a surface weighted average with x the mass-fraction of B, ρ bulk mass density, d particle diameter, and satisfying $S_A + S_B = 1$. Using the measured reflectance of the pure quartz powder sample for R_B , using the vendors data for mean particle diameter and the bulk densities, non-linear least-squares fitting of Equation 2 for R_A and R_A^S provided a poor match to the quartz/KBr powder mixture data.

$$S_B = \frac{x}{x + (1-x) \frac{\rho_B d_B}{\rho_A d_A}} \quad \text{Equation 3}$$

Following on the approach of Schatz, a new formula as given in Equation 4 was developed,

$$R_{\text{mix},\lambda} = 0.5 (1 - x)^2 b_\lambda + 0.5 x(1 - x) c_\lambda R_{B,\lambda} + x R_{B,\lambda} \quad \text{Equation 4}$$

which provided a good match to the quartz/KBr powder mixture data, again using the measured reflectance as a function of wavenumbers of the pure quartz powder sample for $R_{B,\lambda}$, with x the mass-fraction of quartz (B), and non-linear least-squares fits limiting $b_\lambda \approx 1$ and $c_\lambda \approx 1$. In fact, fixing $c_\lambda = 1$ and fitting for $b_\lambda \approx 1$ alone also provides a set of good fits over the whole wavenumber range studied. The functional form proposed by Schatz is the sum of a term scaling as the square of the fraction of the transparent component, a term scaling linearly as the fraction of the absorbing component, and a term proportional to the product of the component's fractions. Contrary to the recommendations of Schatz, mass- rather than surface-fraction provided a better fit to the quartz/KBr powder mixture data, and the coefficient of the cross-term appeared directly proportional to the reflectivity of the strongly absorbing component and not to the index of one component embedded into the other.

Conclusions

A new, high power, tunable QCL-based standoff system is demonstrated that utilizes a lock-in detection scheme with an uncooled MCT detector and a close focus Dall Kirkham telescope. Reflectance spectra are reported for standoff measurements of various sample types including a NIST traceable polystyrene standard reflector, quartz powder, olive oil, and quartz/KBR powder mixtures. This work focused on chemical compounds with strongly absorbing features including

in the presence of non-absorbing mixtures. Several models for reflectance of mixtures were evaluated, and a modified version of the model proposed by Schatz was observed to work well for the mixtures studied. The uncooled MCT detector produced good quality and suitable dynamic range reflectance data at standoff distances of 12.5 m across the spectral range of ~ 1182 to 1000 cm^{-1} (8.45 to $10.03\text{ }\mu\text{m}$). The combination of a solid-state tunable mid-IR QCL modulated at high frequency with an uncooled MCT detector and lock-in signal processing offers the potential for fieldable standoff applications involving chemical identification of neat or mixed compounds.

Acknowledgements

This work was performed under the auspices of the U.S. Department of Energy by Lawrence Livermore National Laboratory under Contract DE-AC52-07NA27344. This document was prepared as an account of work sponsored by an agency of the United States government. Neither the United States government nor Lawrence Livermore National Security, LLC, nor any of their employees makes any warranty, expressed or implied, or assumes any legal liability or responsibility for the accuracy, completeness, or usefulness of any information, apparatus, product, or process disclosed, or represents that its use would not infringe privately owned rights. Reference herein to any specific commercial product, process, or service by trade name, trademark, manufacturer, or otherwise does not necessarily constitute or imply its endorsement, recommendation, or favoring by the United States government or Lawrence Livermore National Security, LLC. The views and opinions of authors expressed herein do not necessarily state or reflect those of the United States government or Lawrence Livermore National Security, LLC, and shall not be used for advertising or product endorsement purposes.

The authors thank Zachary Doorenbos for his help and training in mixing samples using the resonance acoustic mixing (RAM) technique.

References

1. P. Voosen. "NASA's Perseverance Rover Aims To Find Out Whether Ancient Mars Was Warm and Wet or Cold and Dry". *Science*. 2020. 368(6498): 1416-1421.
2. S. Maurice, R.C. Wiens, P. Bernardi, et. al. "The SuperCam Instrument Suite on the Mars 2020 Rover: Science Objectives and Mast-Unit Description". *Space Sci. Rev.* 2021. 217(47): 1-108.
<https://link.springer.com/content/pdf/10.1007/s11214-021-00807-w.pdf> [accessed October 26, 2021]
3. S. Maurice, R.C. Wiens, M. Saccoccio, et. al. "The ChemCam Instrument Suite on the Mars Science Laboratory (MSL) Rover: Science Objectives and Mast Unit Description". *Space Sci. Rev.* 2012. 170: 95-166.
<https://link.springer.com/content/pdf/10.1007/s11214-012-9912-2.pdf> [accessed October 26, 2021]
4. C.W. Van Neste, L.R. Senesac, and T. Thundat. "Standoff Spectroscopy of Surface Adsorbed Chemicals". *Anal. Chem.* 2009. 81(5): 1952-1956.
5. F. Fuchs, S. Hugger, M. Kinzer, R. Aidam, W. Bronner, et. al. "Imaging Standoff Detection of Explosives Using Widely Tunable Mid Infrared Quantum Cascade Lasers". *Optical Engineering*. 2010. 49(11): 111127-1 to 8.
6. J.D. Suter, B. Bernacki, M.C. Phillips. "Spectral and Angular Dependence of Mid-Infrared Diffuse Scattering from Explosives Residues for Standoff Detection Using External Cavity Quantum Cascade Lasers". *Appl. Phys. B.* 2012. 108(4): 965-974.
7. X. Chen, D. Guo, F-S. Choa, C-C. Wang, S. Trivedi, A.P Snyder, G. Ru, J. Fan. "Standoff Photoacoustic Detection of Explosives Using Quantum Cascade Laser and an Ultrasensitive Microphone". *Appl Opt.* 2013. 52(12): 2626-2632.

8. M.E. Morales-Rodríguez, C.W. Van Neste, L.R. Senesac, S.M. Mahajan, T. Thundat. "Ultraviolet Decomposition of Surface Adsorbed Explosives Investigated with Infrared Standoff Spectroscopy". *Sens. and Actuators B*. 2012. 161(1): 961–966.
9. R.C. Sharma, D. Kumar, N. Bhardwaj, S. Gupta, H. Chandra, A.K. Maini. "Portable Detection System for Standoff Sensing of Explosives and Hazardous Materials". *Optics Comm*. 2013. 309: 44–49.
10. X. Liu, C.W. Van Neste, M. Gupta, Y.Y. Tsui, S. Kim, T. Thundat. "Standoff Reflection–Absorption Spectra of Surface Adsorbed Explosives Measured with Pulsed Quantum Cascade Lasers". *Sens. and Actuators B*. 2014. 191: 450–456.
11. A.K. Goyal, T.R. Myers. "Active Mid-Infrared Reflectometry and Hyperspectral Imaging". In: P.M. Pellegrino, E.L. Holthoff, M.E. Farrell. *Laser-Based Optical Detection of Explosives – 1st Edition*. Boca Raton: CRC Press, 2015. Chap. 8, pp. 168-211.
12. I. Chae, M.F. Khan, J. Song, T. Kang, J. Lee, T. Thundat. "Standoff Mechanical Resonance Spectroscopy Based on Infrared-Sensitive Hydrogel Microcantilevers". *Anal. Chem*. 2016. 88(19): 9678–9684.
13. Y. Fu, H. Liu, J. Xie. "100-m Standoff Detection of a QCL-Induced Photo-Vibrational Signal on Explosives Using a Laser Vibrometer". *Opt. Lasers Eng*. 2018. 107: 241-246.
14. M.F. Witinski, R. Blanchard, C. Pfluegl, et. al. "Portable Standoff Spectrometer for Hazard Identification Using Integrated Quantum Cascade Laser Arrays from 6.5 to 11 μm ". *Opt. Express*. 2018. 26(9): 12159-12168.
15. C.J. Breshike, C.A. Kendziora, R. Furstenberg, V. Nguyen, A. Kusterbeck, R.A. McGill. "Infrared Backscatter Imaging Spectroscopy of Trace Analytes at Standoff". *J. Appl. Phys*. 2019. 125(10): 104901-1 to 9.
16. M. Chilenski, C. Murphy, G. Raz. "A Fast Approximation for Adaptive Wavelength Selection for Tunable Infrared Chemical Sensors". *Rev. Sci. Instrum*. 2019. 90(10): 104102-1 to 9.
17. A. Lyakh, R. Barron-Jimenez, I. Dunayevskiy, R. Go, C.K.N. Patel. "External Cavity Quantum Cascade Lasers with Ultra Rapid Acousto-Optic Tuning". *Appl. Phys. Lett*. 2015. 106(14): 141101-1 to 4.
18. L.M. Hansen, C. Zhu. "Wavenumber Standards for Mid-Infrared Spectrometry". In: J.M. Chalmers, P.R. Griffiths. *Handbook of Vibrational Spectroscopy*. Chichester: J. Wiley & Sons Ltd, 2002. Vol. 1, pp. 881-890.
19. M.D Guillen, N. Cabo. "Infrared Spectroscopy in the Study of Edible Oils and Fats". *J. Sci. Food Agric*. 1997. 75: 1-11.
20. N.A. Marigheto, E.K. Kemsley, M. Defernez, R.H. Wilson. "A Comparison of Mid Infrared and Raman Spectroscopies for the Authentication of Edible Oils". *J. Am. Oil Chem. Soc*. 1998. 75(8): 987-992.
21. N. Sinelli, M.S. Cosio, C. Gigliotti, E. Casiraghi. "Preliminary Study on Application of Mid Infrared Spectroscopy for the Evaluation of the Virgin Olive Oil Freshness". *Analytica Chim. Acta*. 2007. 598(1): 128-134.
22. J.M. Ottaway, J.C. Carter, K. Adams, J. Camancho, B. Lavine, K. Booksh. "Comparison of Spectroscopic Techniques for Determining the Peroxide Value of 19 Classes of Naturally Aged, Plant-Based Edible Oils". *Appl. Spectrosc*. 2021. 75(7): 781-794.
23. J. Feng, B. Rivard, D. Rogge, A. Sánchez-Azofeifa. "The Longwave Infrared (3–14 μm) Spectral Properties of Rock Encrusting Lichens Based on Laboratory Spectra and Airborne SEBASS Imagery". *Remote Sens. Environ*. 2013. 131: 173-181.
24. J.F. Mustard, J.E. Hays. "Effects of Hyperfine Particles on Reflectance Spectra from 0.3 to 25 μm ". *Icarus*. 1997. 125: 145-163.

25. E. Rost, C. Hecker, M.C. Schodlok, F.D. van der Meer. “Rock Sample Surface Preparation Influences Thermal Infrared Spectra”. *Minerals*. 2018. 8: 475-496.
26. J.W. Salisbury, A. Wald. “The Role of Volume Scattering in Reducing Spectral Contrast of Reststrahlen Bands in Spectra of Powdered Minerals”. *Icarus*. 1991. 96: 121-128.
27. J.W. Salisbury, L.S. Walter, N. Vergo. “Mid-infrared (2.1-25 μm) Spectra of Minerals: First Edition”. U.S. Geological Survey, Open-File Report 87-263. (1987), pp. 299-300.
<https://pubs.usgs.gov/of/1987/0263/report.pdf> [accessed October 26, 2021]
28. S. Popova, T. Tolstykh, V. Vorobev. “Optical Characteristics of Amorphous Quartz in the 1400–200 cm^{-1} Region”. *Opt. Spectrosc.* 1972. 33: 444-445.
29. M. He, W. Yan, Y. Chang, K. Liu, X. Liu. “Fundamental Infrared Absorption Features of α -Quartz: An Unpolarized Single-Crystal Absorption Infrared Spectroscopic Study”. *Vib. Spectrosc.* 2019. 101: 52-63.
30. H.G. Hecht. “The Interpretation of Diffuse Reflectance Spectra”. *J. Res. Natl. Inst. Bur. Stand. A. Phys. Chem.* 1976. 80A(4): 567-583.
31. H.G. Hecht. “Quantitative Analysis of Powder Mixtures by Diffuse Reflectance”. *Appl. Spectrosc.* 1980. 34(2): 161-164.
32. E.A. Schatz. “Reflectance of Compacted Powder Mixtures”. *J. Opt. Soc. Am.* 1967. 57(7): 941-950.

Figures and Captions

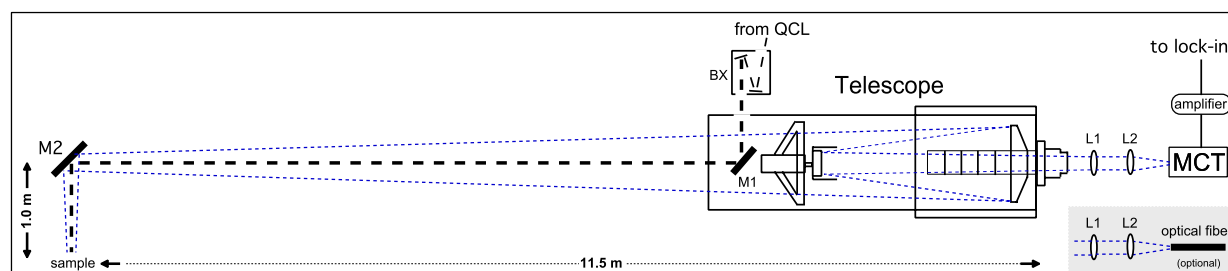


Figure 1. Quantum cascade laser (QCL) based standoff measurements were acquired at a distance of 12.5 m using a large aperture telescope coupled to an uncooled MCT detector with a lock-in amplifier detection scheme. QCL pulses exiting a beam expander (BX) were coaxially aligned with the optical axis of a 10-inch Dall-Kirkham telescope via a fixed mirror (M1) positioned within the telescope extension tube and directed onto a remotely positioned sample via a second fixed mirror (M2) located 11.5 m away (Note: M2 directed the beam downward toward the floor so that samples could be placed horizontal for convenience). Light reflected from the sample to mirror M2 was collected by the telescope and directed to the MCT detector via ZnSe collimating (L1) and focusing (L2) optics. (Inset, grey box) An optical fiber coupled to a HeNe laser (not shown) was positioned where the MCT detector is located during initial alignment to ensure overlap of QCL pulses with the telescope field of view (FOV) and for sizing mirror M2 to be sufficiently large such that the telescope is the limiting aperture.

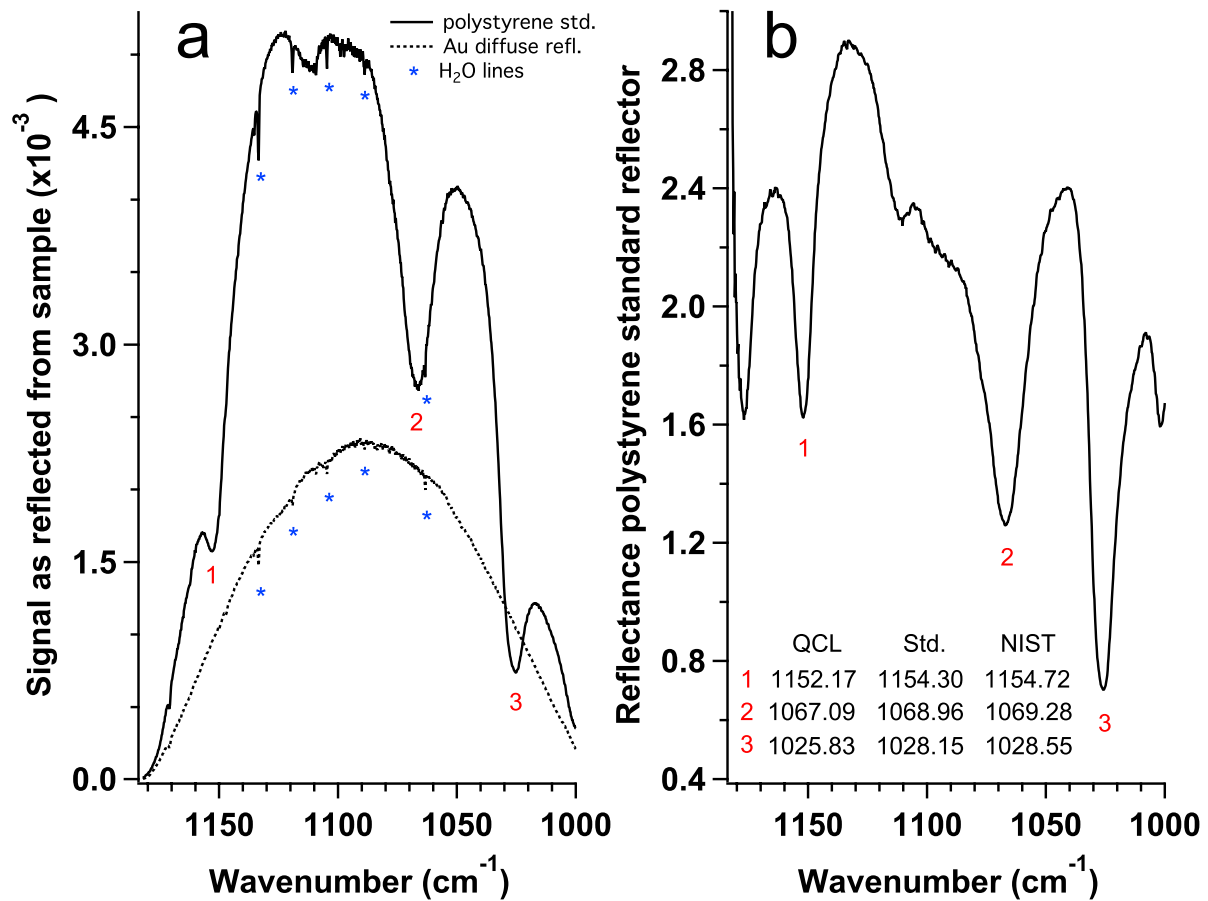


Figure 2. (a, solid trace) The signal as reflected from a NIST traceable polystyrene standard reflector and the (a, dashed trace) signal as reflected from the Au-coated diffuse reflector include (a, *) multiple sharp ambient water lines. The ratio of the (a, solid trace) former with the (a, dashed trace) latter produces the (b) reflectance spectrum of the polystyrene standard reflector and sufficiently removes the water lines and the wavenumber dependent power output profile of the QCL. (1, 2, 3) Polystyrene absorption spectral features were used to determine the QCL tuning range and relative wavenumber position, which varied between -1.87 to -2.32 cm^{-1} , to the polystyrene standard reflector (inset Table, Std. column) calibration data. All measurements were conducted at a distance of 12.5 m using the QCL-based standoff system.

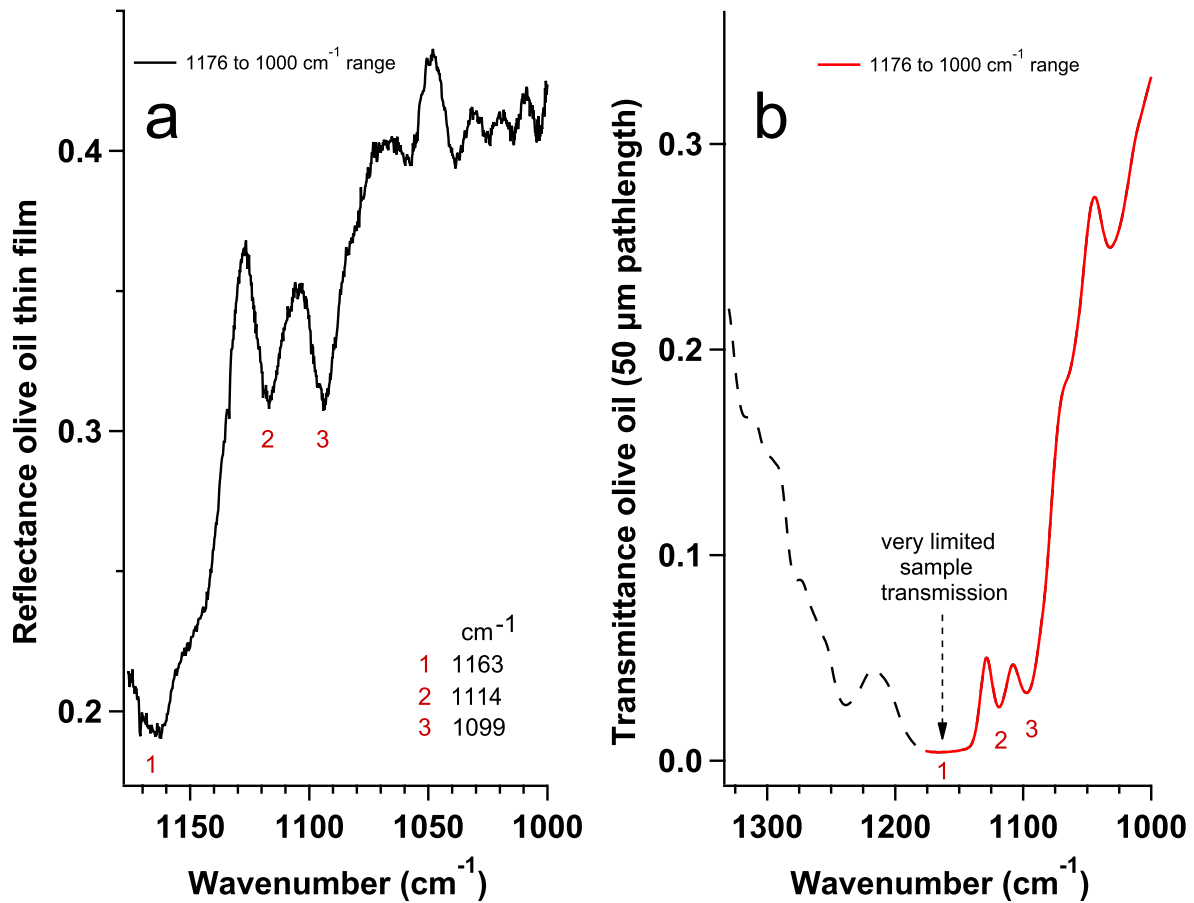


Figure 3. (a) The reflectance spectrum of a thin film olive oil sample is from measurements acquired at a distance of 12.5 m using the QCL standoff system. The limited tuning range of the QCL only allows interrogating a portion of the strong C-O band region having multiple strong (1, 2, 3) absorption features that extend beyond 1330 cm⁻¹ as clearly shown in the (b) transmittance spectrum of olive oil acquired over a broader spectral range using a FT-IR spectrometer (non-standoff).

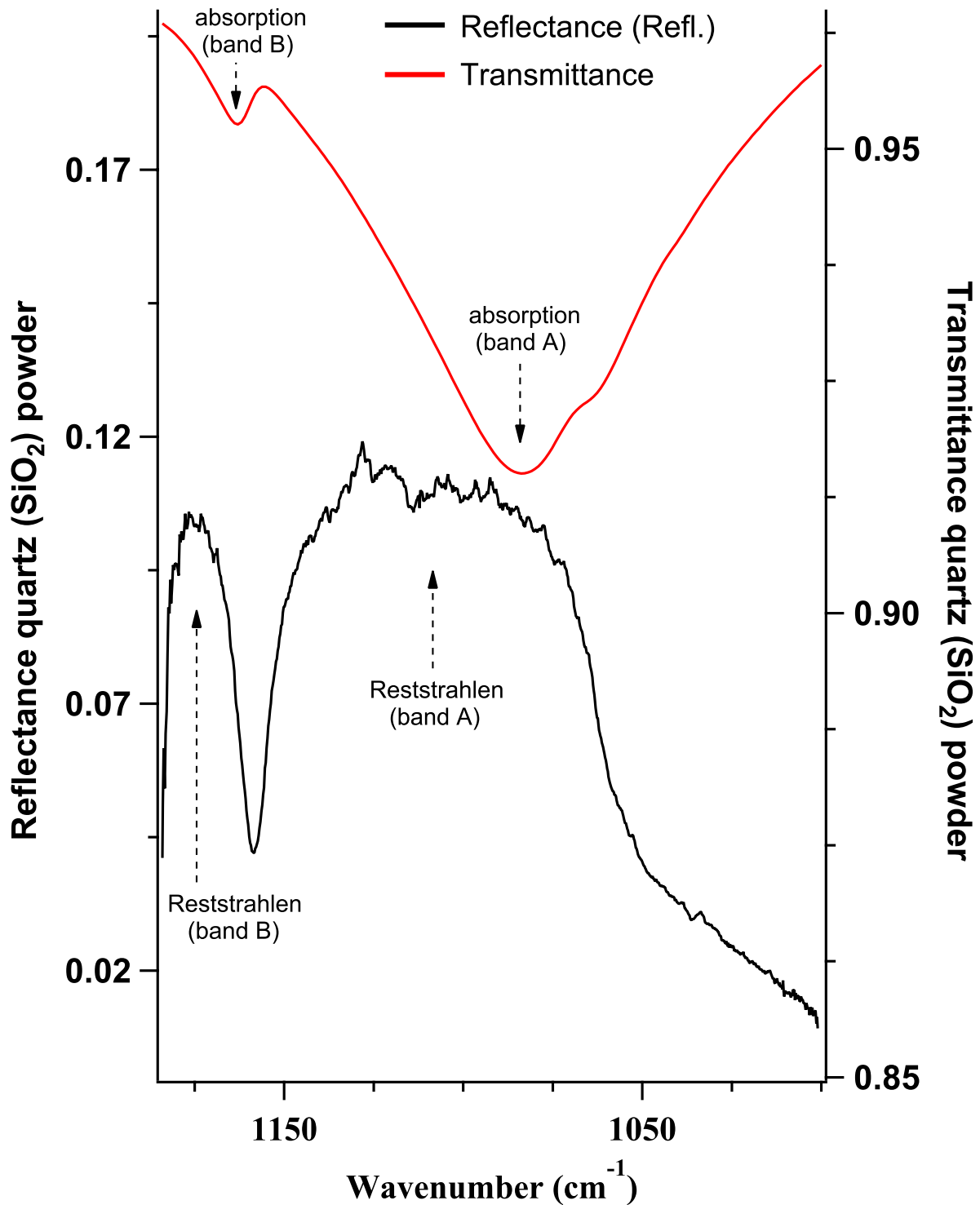


Figure 4. (black trace, left axis) Reflectance and (red trace, right axis) transmittance spectra of bulk quartz powder were acquired from measurements using the QCL-based standoff system (12.5 m distance) and a benchtop FT-IR spectrometer with ATR accessory, respectively. Reststrahlen bands A (1110 cm^{-1}) and B (1175 cm^{-1}) in the reflectance spectrum correspond to absorption bands A (1084 cm^{-1}) and B (1163 cm^{-1}) in the transmittance spectrum.

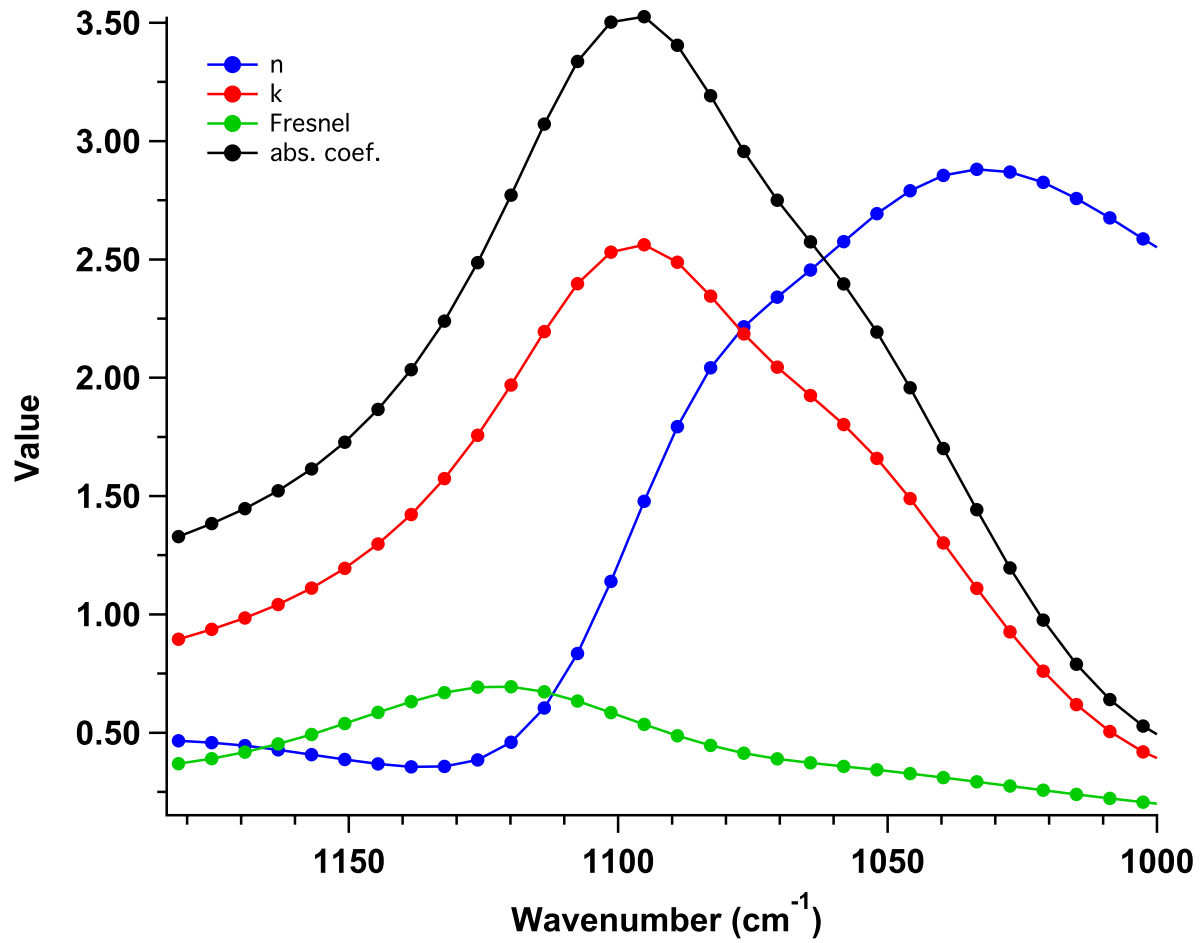


Figure 5. Plots show the (n) real and (k) imaginary parts of the refractive index of quartz along with Fresnel reflection at normal incidence and (α) absorption coefficients in units of $1/\mu\text{m}$. The wavenumber range plotted corresponds to the QCL tuning range.

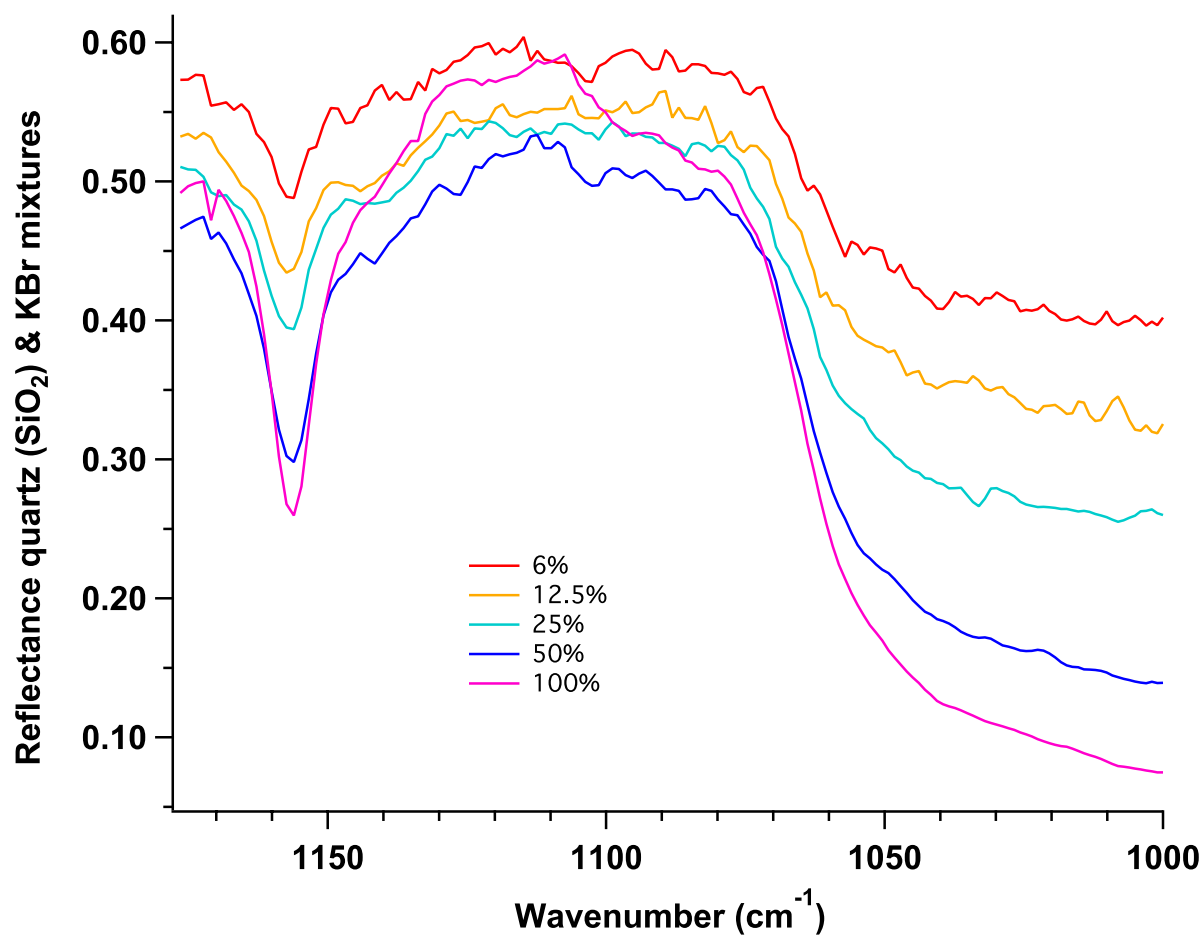


Figure 6. Reflectance of pure quartz powder and powder mixtures of quartz in KBr. The 100% quartz powder reflectance spectrum shown here is from the same data discussed in Figure 4.

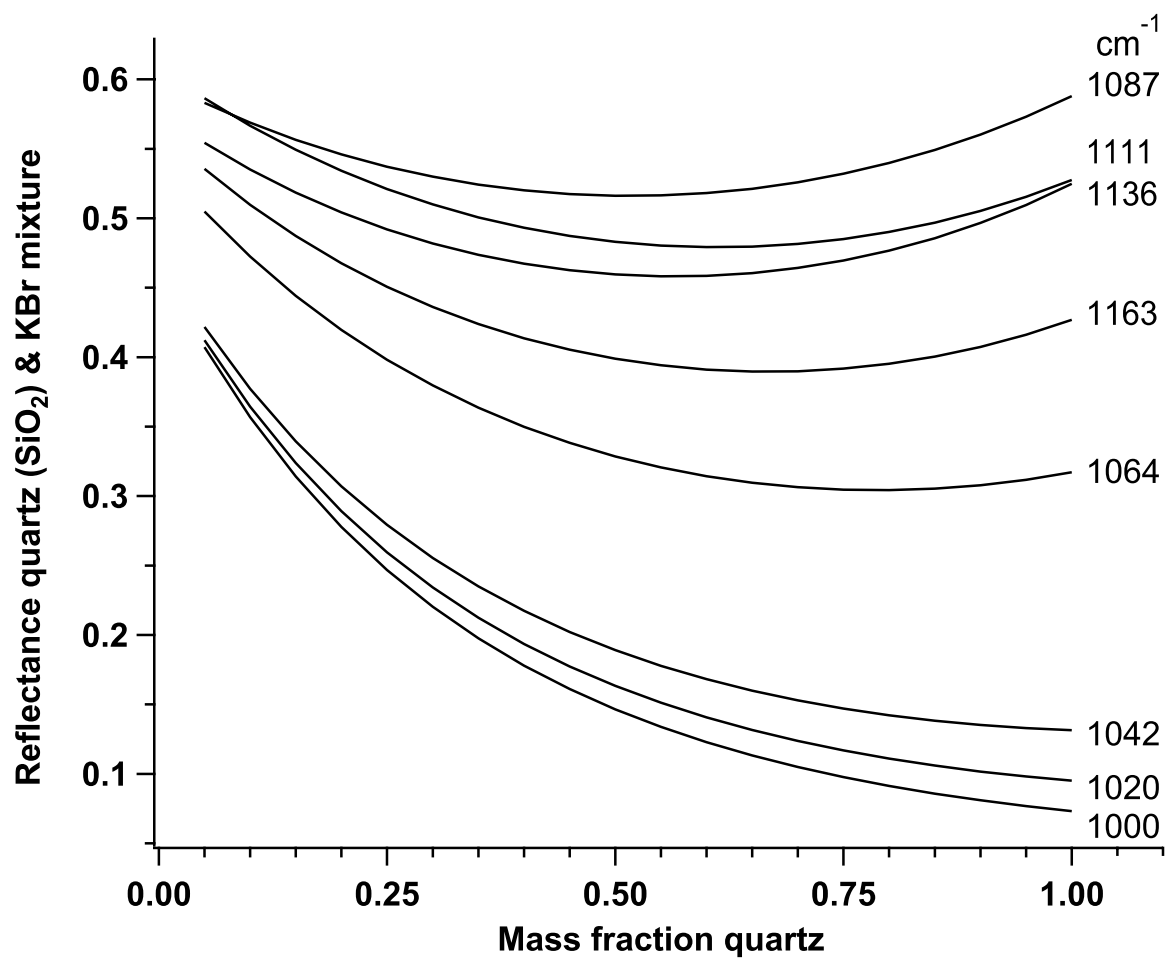


Figure 7. Fits (according to Equation 1) to the measured reflectance are shown at eight select wavenumbers as a function of mass-fraction of quartz powder in KBr powder.